Strain compensation technique in self-assembled InAs/GaAs quantum dots for applications to photonic devices

2009 J. Phys. D: Appl. Phys. 42 073002

(http://iopscience.iop.org/0022-3727/42/7/073002)

IOP Publishing Journal of Physics D: Applied Physics

J. Phys. D: Appl. Phys. **42** (2009) 073002 (12pp) doi:10.1088/0022-3727/42/7/073002

TOPICAL REVIEW

Strain compensation technique in self-assembled InAs/GaAs quantum dots for applications to photonic devices

J Tatebayashi[1], N Nuntawong[2], P S Wong[1], Y-C Xin[3], L F Lester[3] and D L Huffaker[1]

[1] Electrical Engineering, University of California, Los Angeles, 420 Westwood Plaza, Los Angeles, CA 90095, USA
[2] National Electronics and Computer Technology Center, 112 Thailand Science Park, Pathumthani 12120, Thailand
[3] Center for High Technology Materials, University of New Mexico, 1313 Goddard SE, Albuquerque, NM 87106, USA

E-mail: tatebaya@ee.ucla.edu and huffaker@ee.ucla.edu

Received 15 December 2008
Published 20 March 2009
Online at stacks.iop.org/JPhysD/42/073002

Abstract
We report the strain compensation (SC) technique for a stacked InAs/GaAs self-assembled quantum dot (QD) structure grown by metalorganic chemical vapour deposition (MOCVD). Several techniques are used to investigate the effect of the SC technique: the high-resolution x-ray diffraction (XRD) technique is used to quantify the reduction in overall strain, atomic force spectroscopy is used to reveal that the SC layer improves the QD uniformity and reduces the defect density and photoluminescence characterization is used to quantify the optical property of stacked InAs QDs. In addition, experimental and mathematical evaluation of reduction in the strain field in the compensated structure is conducted. We identify two types of strain in stacked QD samples, homogeneous and inhomogeneous strain. XRD spectra indicate that $v_i > 36\%$ reduction in the homogeneous strain can be accomplished. Inhomogeneous strain field is investigated by studying the strain coupling probability as a function of the spacer thickness, indicating that 19% reduction in inhomogeneous strain within SC structures has been evaluated. Next, device application of SC techniques including lasers and modulators is reported. Room temperature ground-state lasing from 6-stack InAs QDs with GaP SC is realized at a lasing wavelength of 1265 nm with a threshold current density of $108\,\mathrm{A\,cm^{-2}}$. The electro-optic (EO) properties of 1.3 μm self-assembled InAs/GaAs QDs are investigated. The linear and quadratic EO coefficients are $2.4 \times 10^{-11}\,\mathrm{m\,V^{-1}}$ and $3.2 \times 10^{-18}\,\mathrm{m^2\,V^{-2}}$, respectively, which are significantly larger than those of GaAs bulk materials. Also, the linear EO coefficient is almost comparable to that of lithium niobate.

1. Introduction

Research on the growth of quantum dots (QDs) and their application to photonic devices including lasers and modulators has received considerable attention due to the prediction that device characteristics would be dramatically improved owing to their unique properties of zero-dimensional systems [1]. Since the first demonstration of QD lasers was reported in 1994 [2], several groups have reported the lasing of QD lasers at $\cong$1.0 μm [2–6]. QDs have recently attracted practical interest since QDs can extend the lasing wavelength of GaAs-based lasers to 1.3 or 1.55 μm, suitable for metro/access optical-fibre communication systems with low threshold current densities (J_{th}), low-chirp operation, high-speed modulation and high J_{th} temperature stability [7–12]. Many groups have realized 1.3 μm continuous-wave (cw) lasing at room temperature (RT) of In(Ga)As/GaAs QD lasers grown by molecular beam epitaxy (MBE) [13–19], and high-performance QD lasers with a high characteristic temperature ($T_0 = 320$ K) [18] or a very low threshold current density ($J_{th} = 16$ A cm^{-2}) [19] have been demonstrated.

QD-based photonic devices grown by metalorganic chemical vapour deposition (MOCVD) have also attracted practical interest in terms of the application to distributed feedback lasers or photonic integrated devices that require regrowth or selective area growth. Moreover, commercialization of QD-based photonic devices would be enhanced by developing the devices grown by MOCVD in terms of high growth rate for mass production. Several groups have so far reported QD lasers grown by MOCVD [20–26]. Lasing near 1.3 μm has been for the first time obtained from 5-stack InAs/InGaP QDs clad by an InGaP layer [21], and recently ground-state lasing has been obtained under cw operation at RT at 1.35 μm, with a maximum ground-state modal gain of 19.3 cm^{-1} [26]. However, the accumulation of the overall compressive strain by stacking In(Ga)As/GaAs QDs can cause threading dislocations as shown in figure 1(*a*) and increases the internal loss due to scattering introduced by undulations of the interface between the active and the p-clad layer. The accumulated strain fields also cause a reduced QD density due to seeding effects from the progressive size of stacked QDs.

One of the ways to circumvent these problems is to insert a tensile layer within the stacked structure to compensate the overall compressive strain. In compressive strained quantum well (QW) lasers, the compensation of compressive strain by inserting tensile layers has been demonstrated using InGaP and InGaAsP. Improvements in both crystalline quality and lasing performance including higher photoluminescence (PL) intensity, narrower PL linewidth and lower threshold current density have been proven [27–29]. In stacked QD active regions, the use of the strain compensation (SC) technique would be a powerful parameter in designing laser structures to reduce defect formation and compensate the compressive strain. Two methods for compensating the overall strain of stacked QDs have been reported. One approach is to use GaNAs SC as the capping layer of InAs QDs [30], and another is to insert Ga(In)P SC layers within the stacked structure [24, 31–33] but, so far, this SC technique has not been well studied. The lack of studies on phosphide-based materials is likely due to the inconvenience of a pyrophoric phosphide source in QD-growing MBE systems. We have already reported the effect of SC in stacked InAs QDs [32, 33] and demonstrated the lasing at 1.265 μm from multi-stacked InAs QDs with GaP SC layers with the threshold current density of 108 A cm^{-2} [24, 25].

In this paper, we closely investigate a SC technique to improve both the structural and the optical properties of stacked InAs QDs grown by MOCVD. First, fabrication of stacked InAs QDs with a thin GaP tensile layer embedded in GaAs barriers to reduce the accumulation of compressive strain in the stacked InAs QD active regions is investigated. The effects of the SC layers are investigated by using several

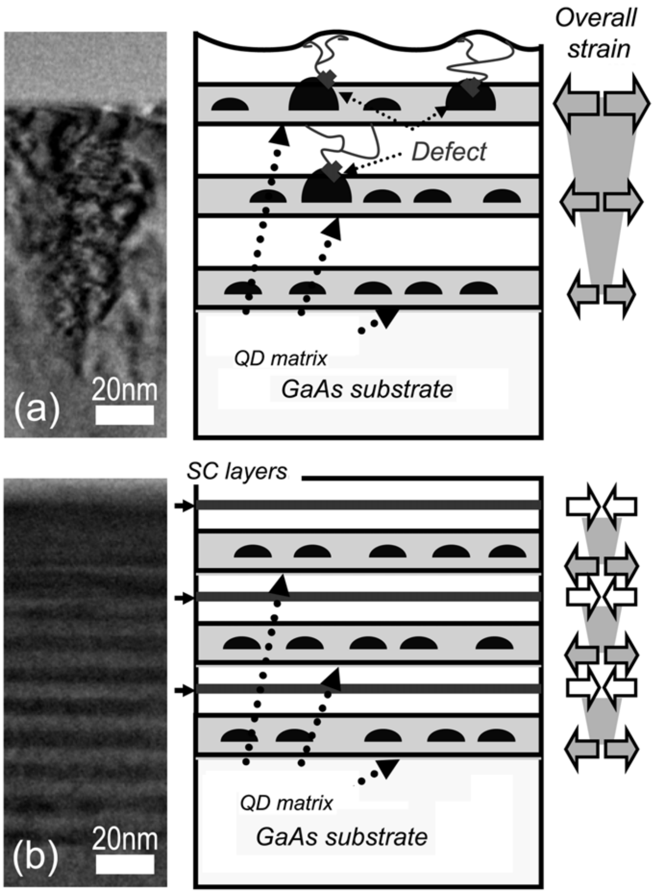

Figure 1. Cross-sectional TEM image and schematic illustration of a 10-stack QD grown by MOCVD with a spacer thickness of 15 nm (*a*) without and (*b*) with a GaP SC layer.

methods. Atomic force spectroscopy (AFM) reveals that the SC layer improves the uniformity of InAs QDs and reduces the defect density. PL is used to corroborate the improved optical properties. Next, we identify two types of strain in QD structures, homogeneous and inhomogeneous strain. High-resolution x-ray diffraction (XRD) spectra are used to quantify the homogeneous strain. The inhomogeneous strain field is investigated by studying the strain coupling probability as a function of the spacer thickness. Then, the device applications of the SC technique including lasers and modulators are reported. We investigate the device properties including the threshold current density (J_{th}), the lasing spectra, the modal gain and the internal loss of a laser with a 6-stack InAs/GaAs QD active region utilizing 6 monolayer (ML) GaP SC layers embedded in 27 nm GaAs spacers. For the modulator application, the electro-optic (EO) properties of stacked InAs/GaAs QDs with GaP SC are studied. The linear EO (LEO) and quadratic EO (QEO) coefficients are quantified by measuring the phase retardation characteristics of the fabricated QD modulators.

2. Sample growth and characterization of stacked InAs QDs with SC

In general, accumulation of strain is a limiting factor in the epitaxial growth of a lattice-mismatched material system. For bulk materials, the thickness at which the strained crystal starts developing the misfit dislocations is defined as the critical thickness [34]. Above the critical thickness the minimum energy is achieved through the introduction of dislocations and lattice relaxation. Relaxation implies that the material that has been once strained and contorted now comes back to its original lattice size. In the strained multiple QW or QD structures, strain accumulates and the critical thickness can be reached as the number of strained layers increases.

Figure 1(*a*) shows the bright-field cross-sectional transmission electron microscopy (TEM) image of a 10-stack QD structure using the growth condition of a single-stack QD with an emission wavelength of 1.3 μm. The QD layers are separated by 15 nm GaAs spacers. The accumulation of compressive strain through these thin spacer structures results in dislocation formation and relaxed surface. The quality of this sample is much lower than those in any working QW or QD devices. Indeed, the QD structure with this high dislocation density is not expected to emit any light from the active region at all. In order to avoid the relaxation, the total elastic energy, E_{total}, of the structure must be less than a critical value. The relationship between the total elastic energy as a function of the number of stacks, N_{stacks}, and the average strain can be described as [35]

$$E_{\text{total}} \propto N_{\text{stacks}} \langle \varepsilon_{\perp} \rangle^2 t_{\text{spacing}}, \quad (1)$$

where $\varepsilon_{\perp}$ and t_{spacing} are the average strain of each QD layer including GaAs barriers and the thickness of the spacers, respectively. So far, two materials have been reported for compensating the compressive strain in InAs/GaAs QDs, one is to use the binary material GaP and the other is to use the ternary material InGaP. The improved crystalline quality using InGaP SC layers has been verified [32]. However, the InGaP layers can lead to bimodal size distribution of QDs and phase separation at the InGaP/GaAs interface under HRTEM. For these reasons, the binary GaP material is certainly a better choice of SC material than ternary InGaP. However, the thickness of the GaP layer has to be optimized due to the large lattice mismatch between GaP and GaAs.

2.1. Sample preparation and characterization method

All samples are grown in a low-pressure MOCVD system, using trimethylindium (TMI), trimethylgallium, trimethylaluminum, tertiarybutylphosphine and arsine (AsH_3) as the source materials, at a total pressure of 60 Torr. Disilane and carbon tetrachloride are used as the n- and p-type doping materials for laser structures. Growth is initiated on a GaAs (0 0 1) substrate with a 3000 Å GaAs buffer layer grown at 680 °C and then the temperature is reduced and stabilized for active region growth within the range 450–520 °C. Each QD layer consists of a 5 ML $In_{0.15}Ga_{0.85}As$ buffer layer, 3 ML InAs QD coverage and a 25 ML $In_{0.15}Ga_{0.85}As$ capping layer to extend the emission wavelength. An AsH_3 pause is introduced after the growth of each QD layer to reduce the defect density. Stacked QD layers are separated by two GaAs barrier layers sandwiching either a thin GaP SC layer of different thickness, ranging from 2 to 8 MLs, or a 8 ML $In_xGa_{1-x}P$ layer with different compositions ($x = 0.3$ and 0.36) for comparison with GaP SC layers. The lattice constant, a_0, of GaP is $a_0 = 0.545$ nm, resulting in a lattice mismatch of −3.54% to GaAs. The surface characteristics, optical property and crystalline quality of these samples are characterized by using AFM, XRD, TEM and conventional PL with a 5 mW He–Ne laser and a 1.5 mm spot size.

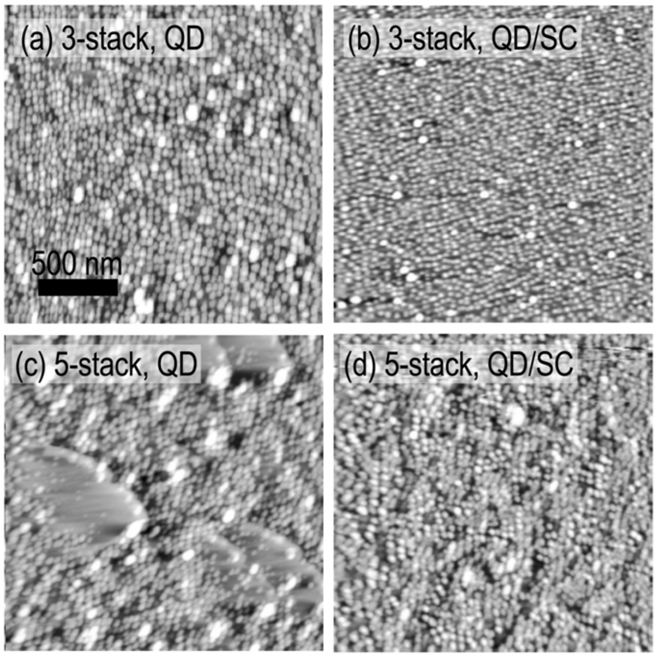

Figure 2. AFM images (2 μm × 2 μm) showing the top layer of a 3-stack (*a*) without SC and (*b*) with SC and a 5-stack (*c*) without SC and (*d*) with SC [24].

2.2. PL and AFM characteristics of stacked with different thicknesses of SC layer

Figure 2 shows AFM images (2 × 2 μm^2) of the surface QD layer atop (*a*), (*b*) a 3-stack and (*c*), (*d*) a 5-stack active region both with and without 4 ML GaP layers. There are several competing effects that control the QD formation under the presence of strain. The general trends are elucidated in table 1. With increased stacking layers, the QD density reduces and the defect density, the QD height and QD diameter increase. The deleterious effects of stacking are reduced by the introduction of SC layers. In more detail, the QD density can remain constant at $\sim 5 \times 10^{10}$ cm^{-2} as the stacking increases if SC is incorporated. Without SC, the vertical overlap of propagating strain fields will likely control the QD nucleation and reduce the QD density. The defect density of the samples without SC increases as the QD density reduces. The 5-stack sample without SC (sample (*c*)) has a high defect density of 2.1×10^9 cm^{-2} and surface undulations. With SC, the defect density remains in the 10^8 cm^{-2} regime. Increased stacking also causes larger QDs in both width and height, compared with a single QD layer. The diameter increases by ∼30% for the samples without SC due to a reduced wetting layer (WL) thickness (more material in the QDs), but only by ∼10% with

Table 1. Tabulated AFM data from the samples in figure 2 including the dot density, the defect density and the dot size for a single layer, 3-stack and 5-stack active regions with and without GaP SC layers [24].

		Dot density (cm^{-2})	Defect density (cm^{-2})	Diameter (nm)	Height (nm)
Single layer	—	5.4×10^{10}	4.0×10^{8}	32	5.5
3-stack layer	without GaP	4.8×10^{10}	9.0×10^{8}	36	5.9
	with GaP	5.1×10^{10}	6.0×10^{8}	31	6.0
5-stack layer	without GaP	2.8×10^{10}	2.1×10^{9}	42	7.3
	with GaP	4.9×10^{10}	6.5×10^{8}	35	7.5

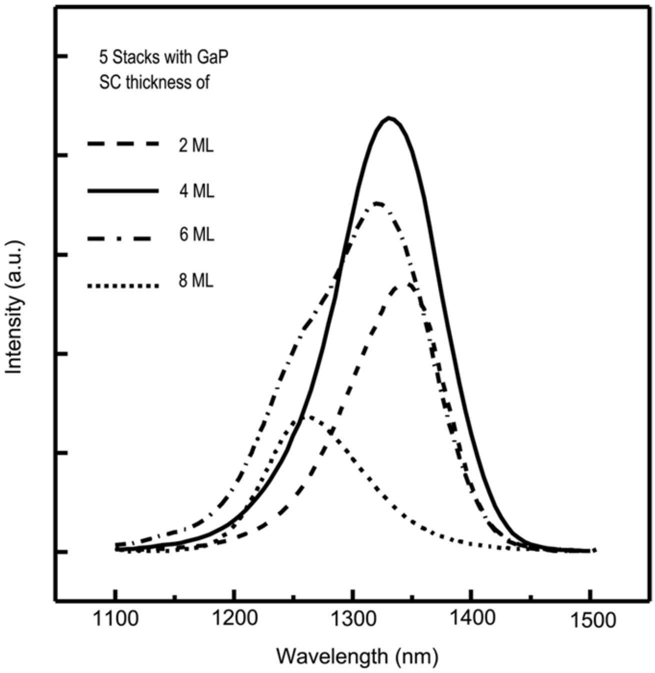

Figure 3. RTPL from the 5-stack samples with 2, 4, 6 and 8 MLs of the GaP SC layer [24].

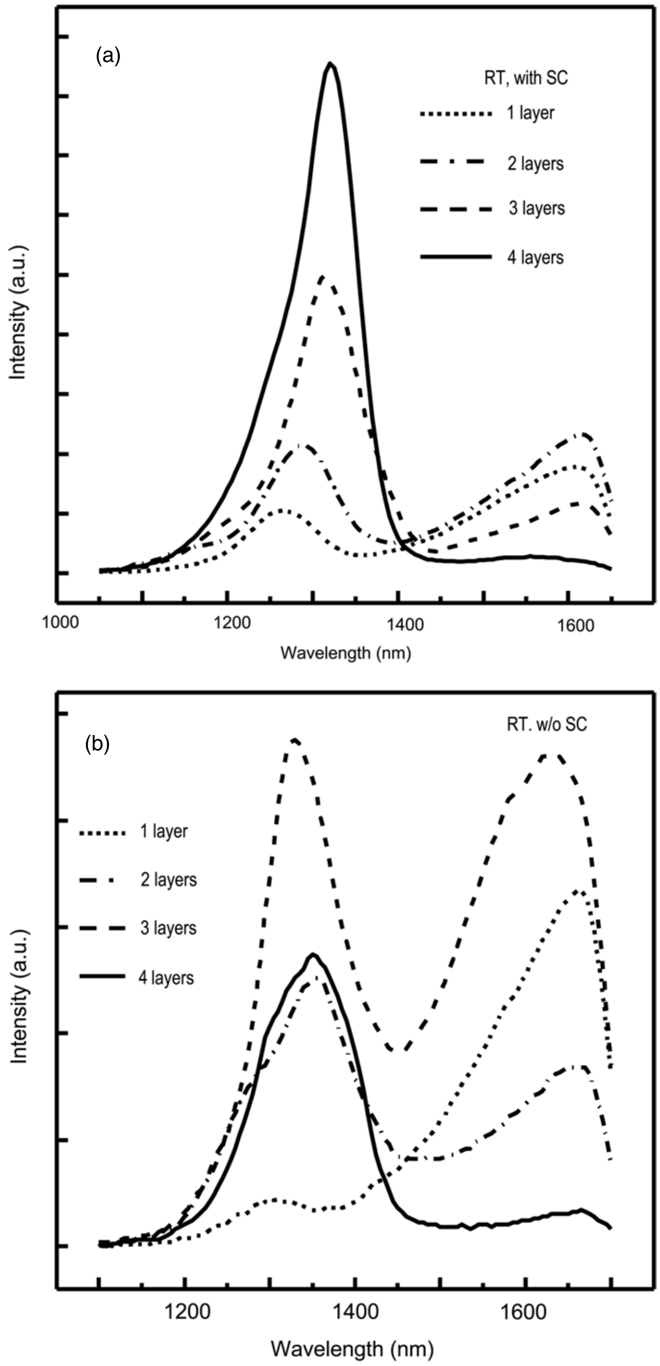

Figure 4. RTPL spectra comparing single to 4-stack QD active regions (*a*) with 4 ML GaP SC and (*b*) without SC layers [24].

SC. The average QD height increases by ∼35% both with and without SC.

Figure 3 shows the RTPL from the 5-stack QD samples with GaP SC layers of different thicknesses: 2, 4, 6 and 8 MLs. Overall, the PL intensity is more than one order of magnitude higher with GaP SC layers than without. As the thickness of the GaP layer increases, a blue shift from 1.33 to 1.25 μm can be observed. This is a result of a 9% reduction in the QD size driven by the increased tensile strain. The PL intensity increases with the GaP layer thickness from 2 MLs to 4 MLs and then decreases for thicknesses of 6 MLs and 8 MLs. The decrease in the PL intensity associated with the thicker GaP SC can be attributed to partial relaxation of the SC layer and dislocations in the structure. The critical thickness of the embedded GaP layer is expected to be much lower than the value reported for GaP on GaAs (∼12 MLs) due to the existing strain from the QD regions.

2.3. PL and AFM characteristics of stacked QDs with different stacking numbers

Figures 4(*a*) and (*b*) show RTPL spectra from four uncapped QD samples with different stacking numbers with SC and without SC, respectively. Two different peaks are identified in each spectrum: one peak at 1.6 μm from the surface QDs and another peak at 1.3 μm from the capped QD region. The electron–hole pairs are mainly generated in the GaAs buffer

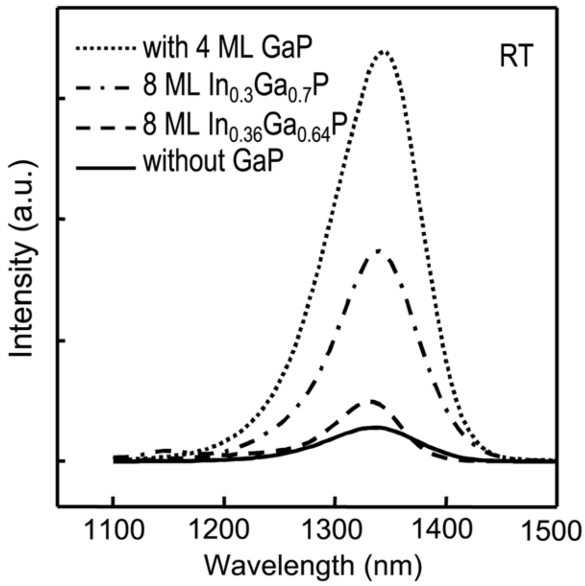

Figure 5. RTPL spectra comparing the QD active regions with (a) GaP, (b) (c) $In_xGa_{1-x}P$ SC and (d) without SC layers in the 5-stack sample.

layer since the GaAs barriers between the QD actives are very thin. In both types of samples (with and without SC) the relative intensity of the uncapped QDs to the capped QDs reduces with additional stacks as more carriers are captured by capped QDs. In figure 4(*a*), the PL intensity increases linearly with each additional QD stack indicating that the number of non-radiative recombination sites does not increase drastically with stacking. The red shift in the PL peak position with the increased number of stack layers is attributed to the increase in the QD size as observed by AFM. In figure 4(*b*), the intensity increases from a 1-stack to a 3-stack, then begins to reduce as the 4th stack is added. The intensity from the single QD stack is fairly low because carriers readily thermalize to the ground state of the surface QDs, where they recombine radiatively and emit at 1.6 μm.

2.4. PL characteristics of stacked QDs with GaP and InGaP SC

Figure 5 shows the improved RTPL intensity of the 5-stack QD structures embedded with the previously optimized 4 ML GaP SC layers compared with a series of samples with InGaP SC. The emission wavelengths are observed between $\lambda = 1340$ nm and $\lambda = 1325$ nm. The comparison shows that the PL intensity with SC is increased by factors of 1.8 (8 ML $In_{0.36}GaP$), 6.2 (8 ML $In_{0.30}GaP$) and 12.5 (4 ML GaP) compared with the sample without SC as a result of fewer non-radiative recombination centres. The full-width at half-maximum (FWHM) varies slightly from sample to sample within the range 58–70 meV. It should be noted here that one of the interesting points in these PL spectra is the comparison between the PL intensities of samples (a) and (b). Although these two samples have a similar amount of strain reduction, the PL intensity of sample (a) is brighter than that of sample (b) by about a factor of 2. This is due to the difference in the material uniformity of InGaP and GaP SC layers due to segregation issue of indium adatom.

3. Strain distribution analyses in stacked QDs

Strain in stacked QD can be categorized into two types, homogeneous (net) strain and inhomogeneous (localized) strain. The difference between these components is their propagating field configurations. The homogeneous strain is initiated from WLs and InGaAs caps, propagating uniformly into GaAs barriers. This homogeneous strain is similar to the strain configuration in the QW structure and can be simply calculated by taking into account the different lattice parameters of the layers, the indium composition and the layer thickness. Compared with the homogeneous strain, the inhomogeneous strain field configuration is more complicated. The inhomogeneous strain originates from embedded QDs propagating into GaAs barriers and is very strong at the QD site, but reduces in strength with vertical propagation. These properties of the inhomogeneous strain make it more difficult to compensate by SC layers, which is evident from the vertical coupling QDs within the structures with SC layers. Although partial compensation of inhomogeneous strain is evident from the reduction in the defect density and the improved QD uniformity, it is important to quantify inhomogeneous strain field compensation.

3.1. Analyses of homogeneous SC

One of the essential tools to characterize heteroepitaxial structural parameters is XRD. By analysing parameters such as peak separation and intensity from the diffraction, structural information such as layer thickness, composition (for a ternary layer) and crystalline tilt can be determined, and they are often complementary to the information obtained from TEM images or from luminescence spectroscopy data. The key strength of the XRD technique is the high strain sensitivity. For epitaxial alloy layers, the lattice strain contributes mostly to the coherent Bragg diffraction. For strained coherent epitaxial layers and the interfaces of common heterostructures, high-resolution XRD with double crystal diffraction (DCD) is capable of providing structural information on the homogeneous strain of the structure. In this system, the measured intensity is an integrated intensity, integrated over the diffraction plane normal to the diffractometer axis that contains the source and the detector.

A series of 5-stack QD samples with $In_xGa_{1-x}P$ SC layers with different In compositions ranging from $x = 0$ to $x = 0.36$ have been grown. A previously optimized thickness which gives the maximum RTPL intensities for each SC composition is used for this experiment. High-resolution XRD is performed using a Philips MRD double-axis diffractometer, employing Cu $K_{\alpha 1}$ ($\lambda = 1.54$ Å) with a four crystal Ge(2 2 0) monochromator and a channel cut Ge(2 2 0) analyzer. Experimental symmetric scans around the (0 0 4) reflection in $\omega/2\theta$ geometry are used to measure the effect of the SC layers on the strain accumulation and the lattice distortion in these stacked QD samples. The XRD spectra for four samples

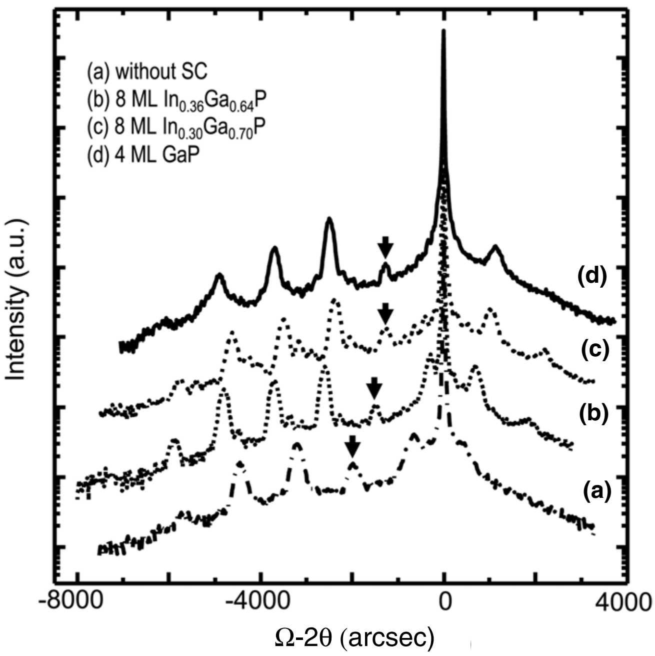

Figure 6. Symmetric 0 0 4 XRD patterns for a 5-stack QD structure with (a) no SC layer, (b) 8 ML $In_{0.36}GaP$, (c) 8 ML $In_{0.36}GaP$ and (d) 4 ML GaP.

that have 5-stack QDs with a spacing thickness of 15 nm and (a) no SC, (b) 8 ML $In_{0.36}GaP$ SC, (c) 8 ML $In_{0.36}GaP$ SC and (d) 4MLs GaP SC structures are shown in figure 6. These four spectra are characterized by zero-order peaks located at (a) $\Delta\theta = -1962$ arcsec, (b) $\Delta\theta = -1476$ arcsec, (c) $\Delta\theta = -1283$ arcsec and (d) $\Delta\theta = -1264$ arcsec. The zero-order peaks in figures 6(*b*)–(*d*) shift closer to the GaAs substrate peak, which indicates reduced compressive strain with decreasing In content in the SC layers.

The average perpendicular strain, $\langle\varepsilon_\perp\rangle$, can be determined by

$$\langle\varepsilon_\perp\rangle = \frac{\sin\theta_B}{\sin(\theta_B + \Delta\theta)} - 1, \tag{2}$$

where θ_B is the Bragg angle of the GaAs substrate. From equation (2) and the experimental values for $\Delta\theta$, we calculate the total strain in each sample and list them in table 2. In these samples, the perpendicular strain, $\langle\varepsilon_\perp\rangle$, varies from 0.014 897 (with no SC) to 0.009 68 (with 4 ML GaP SC), which can be translated to 25–36% reduction in the compressive strain due to the SC layers compared with the sample without SC layers. The total average strain values obtained from the XRD spectra show a total strain reduction of 36% from the structure with 4 ML GaP SC layers, compared with the structure without the SC layer. The results are consistent with the simulation based on a simple model of average perpendicular strain (homogeneous strain) in a QW structure. The strain in this structure can be given by

$$\langle\varepsilon_\perp\rangle = \frac{\sum_i (\varepsilon_\perp)_i \cdot t_i}{\sum_i t_i}, \tag{3}$$

$$\varepsilon_\perp = \frac{a_i - a_{GaAs}}{a_{GaAs}}, \tag{4}$$

where $\varepsilon_\perp$ and t are the strain and the thickness of the ith layer (not including the InAs QD island), respectively, and a_i is the lattice parameter of the ith layer which depends on the material composition. The calculation results from equation (3) are included in table 2. The comparison between the strain reduction values obtained from this model and from the XRD measurement verifies the reduction in the homogeneous strain obtained from the XRD measurement.

3.2. Analyses of inhomogeneous SC

While the effect of SC layers on homogeneous strain reduction has been shown to be obtained from the high-resolution XRD measurements, XRD is limited in information regarding the randomly distributed strain fields produced by QDs (inhomogeneous strain) since they attribute to incoherent, diffuse scattering of the x-ray signal rather than diffraction. The inhomogeneous strain field configuration is thus more complicated to analyse than the homogeneous strain. Instead of the XRD technique, many groups have investigated the strain effect of stacked QDs by varying the spacer thickness [36–39]. An analytical description of the correlated island formation under strain fields has been provided by Xie *et al* [38]. This group has shown that self-assembled QDs induce a tensile strain field in the prospective cap layer grown above the islands. When $t_s < 50$ nm, which is within the strain dependent or strain coupled range, the inhomogeneous strain fields provide the driving force for vertically aligned QD formation. When $t_s > 50$ nm, the inhomogeneous strain field becomes diffused and negligible. Subsequent indium deposition produces island formation that is independent of the underlying QDs and thus strain-decoupled. The occurrence of strain coupling between adjacent QD layers can be observed and evaluated from microscopy images. Hence, it is possible to quantify inhomogeneous strain field within stacked QD structures by evaluating the strain coupling probability of QD formation as a function of the spacer thickness, with and without SC.

In this study, the effect of inhomogeneous strain in stacked QDs with SC layers will be verified by evaluating the vertical coupling probability of QD formation between stacks. Two sets of 5-stack QD samples are grown with varying spacer thicknesses, ranging from 15 to 45 nm, without SC and with 4 ML GaP SC layers. For samples with SC layers, the SC layer is located at 4 nm above each QD layer as in previous studies. In these samples, the InGaAs caps are removed from the QD layers in order to improve the contrast between the QD and GaAs barriers in cross-sectional HRSEM images. Figure 7 shows the [0 1 1] cross-sectional SEM images of the sample with $t_s = 25$ nm (*a*) without and (*b*) with SC layers. From the material contrast, the structure without the SC layers shows a strong coupling between the QD layers. The size of QDs increases by approximately 20% in both width and height by stacking QDs, as shown in figure 7(*a*) under the effect of accumulated inhomogeneous strain in the columnar direction. By counting the number of coupled QDs with the higher magnification image as shown in figure 7(*c*), we obtain a coupling probability of 0.89 for this sample. With the presence of SC layers as shown in figure 7(*b*), the coupling

Table 2. Tabulated XRD data including a zero-order peak, total strain, % strain reduction for 5-stack QDs with a spacer thickness of 15 nm [32].

Data	No SC	$In_{0.36}Ga_{0.64}P$ (8 MLs)	$In_{0.30}Ga_{0.70}P$ (8 MLs)	GaP (4 MLs)
$\Delta\theta$ (arcsec)	−1962	−1476	−1283	−1264
$\langle\varepsilon_\perp\rangle$	0.014 897	0.011 16	0.009 68	0.009 52
Strain reduction (%) (Experiment)	—	25	35	36
Strain reduction (%) (Calculated)	—	33	39	35

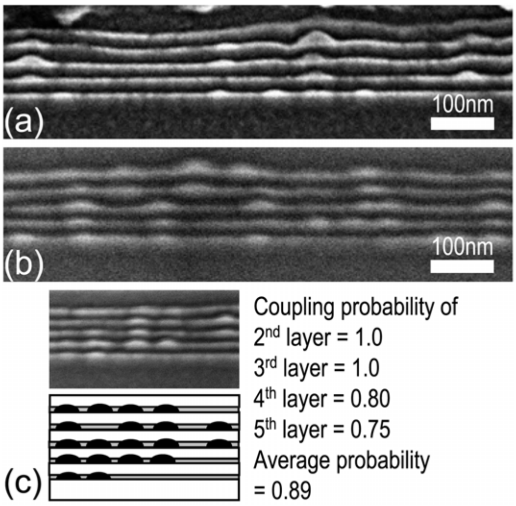

Figure 7. Cross-sectional SEM images of the 5-stack QD ensemble with $t_s = 25$ nm (*a*) without SC and (*b*) showing reduction in the coupling probability with SC layers [39].

probability reduces to 0.70 with improved size uniformity of QDs. The inset of figure 7(*b*) shows evidence of strain-decoupled QD formation at the 4th layer, which suggests successful compensation of the inhomogeneous strain field with SC layers.

Figure 8 shows a schematic illustration of the indium atom migration process on a stressed surface. Under the assumption of an isotropic crystal, where the strain interacts in the same manner regardless of the crystal orientation, the two-dimensional inhomogeneous strain component on the surface along the x-axis can be expressed by [36]

$$\varepsilon_{xx}^{\mathrm{GaAs}}(x, t_s) = 2A\varepsilon_0 \frac{r_0^3}{(x^2 + t_s^2)^{3/2}} \tag{5}$$

and

$$A = \frac{3B_{\mathrm{InAs}}}{3B_{\mathrm{InAs}} + 2E_{\mathrm{GaAs}}/(1 + \upsilon_{\mathrm{GaAs}})} = 0.572, \tag{6}$$

where r_0 is the radius of the equivalent spherical QD, t_s is the barrier thickness and ε_0 (~0.07) is the lattice mismatch between InAs and GaAs. This equation indicates the existence of a strong inhomogeneous strain field at the QD site, which reduces in intensity with vertical propagation. The strain field from a buried QD introduces an inhomogeneous distribution of the surface chemical potential. The surface chemical potential

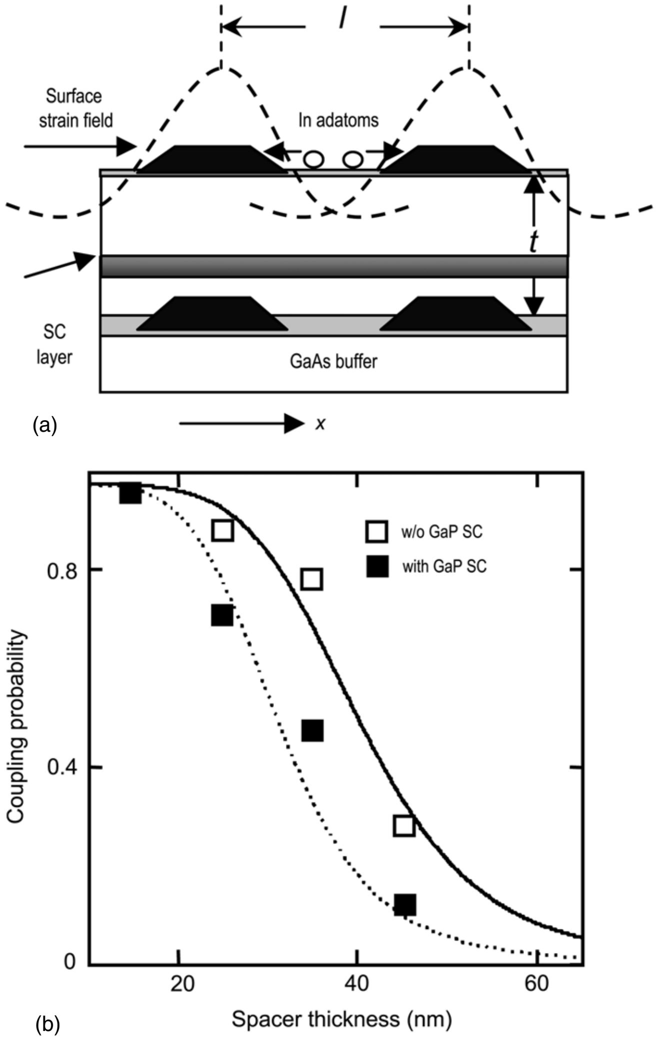

Figure 8. (*a*) Schematic illustration showing the indium atom migration process on the stressed surface. (*b*) Experimental (squares) and simulation (line) results of coupling probabilities as a function of the spacer thickness [39].

for InAs as a function of strain on a flat GaAs surface can be described as [40]

$$\mu(x, t_s) = \mu_0 + \frac{\Omega_{\mathrm{InAs}}}{2E_{\mathrm{InAs}}}\sigma_\tau^2, \tag{7}$$

where μ_0 is the surface chemical potential of bulk InAs, Ω_{InAs} is the atomic volume of an InAs molecule and σ_τ is the tangential stress at the surface. The strain-driven adatom migration generates the net probability of indium atoms being sucked into the regions $-d/2 < x < d/2$ on top of a QD. This net probability K can be expressed as

$$K = \frac{D}{k_B T} \frac{\mu(l/2, t_s) - \mu(0, t_s)}{l/2}, \tag{8}$$

where D is the surface diffusion coefficient of indium adatoms, k_B is the Boltzmann constant, T is the growth temperature,

$$\frac{\mu(l/2, t_s) - \mu(0, t_s)}{l/2}$$

represents the average driving force, $D/k_B T$ is the mobility of the indium adatoms and l is the average separation between QDs. The indium adatom concentration and the amount of material M arriving within $-d/2 < x < d/2$ can be given by [41]

$$n(\pm d/2) = F \times L_D \frac{\sinh Q}{K \cosh Q + V_D \sinh Q} \tag{9}$$

and

$$M = Fd + Kn(d/2) + Kn(-d/2), \tag{10}$$

where F is the indium flux, L_D is the diffusion length, $V_D = L_D/\tau$ (τ is an average incorporation lifetime of indium adatoms) and $Q = (l-d)/2LD$. The pairing probability can be defined as the ratio $P = M/M_T$, where M_T is the total material delivered in unit time within length l. From equations (5)–(10), the probability of QD formation on top of a buried QD depends on the distribution of the surface chemical potential, which is a function of the average lateral separation between QDs (l). The coupling probability is proposed by Xie *et al* [38]:

$$P(t_s) = \frac{d}{l} + \left(1 - \frac{d}{l}\right)\frac{1}{Q} \times \frac{\sinh Q}{\cosh Q + \dfrac{t_s}{r_0^3}\dfrac{l}{8L_D A}\dfrac{2E_{InAs}k_B T}{\Omega_{InAs}(xC_{11}^{InAs}\varepsilon_0)^2}\dfrac{I}{I-1}\sinh Q} \tag{11}$$

and

$$I = (l^2/4t_s^2 + 1)^{3/2}, \qquad Q = (l-d)/2L_D, \tag{12}$$

where the QD widths $d \sim 30$ nm and $l \sim 100$ nm are determined by AFM characterization. The variable x represents the coefficient of the strain field initiated from a buried QD to the upper surface and $x = 1.0$ for a structure without a SC layer.

The coupling probability of these samples obtained from SEM as a function of the spacer thickness is shown in figure 8(*b*). There is no difference in the coupling probabilities between the strain-compensated and uncompensated structures for closely stacked QDs ($t_s < 15$ nm), where the coupling probability is approximately 100% for both cases. For a thicker spacing ($t_s > 25$ nm), the inhomogeneous strain field is partially suppressed by the SC layer and results in the reduction in the coupling probability. By combining equations (5)–(10) and using a diffusion length $L_D \sim 280$ nm, [38], we can treat r_0 of equation (5) as the only unknown. The value of $r_0 = 6.1$ nm is found to be a reasonable fit with our experimental results of the structure without SC (solid), as shown in figure 8(*b*). By using the same parameters and fitting to the SC data while treating x as unknown, we obtain $x = 0.81$. This x value indicates a 19% reduction in the inhomogeneous strain field under the presence of SC layers. This amount of strain reduction is approximately half of the homogeneous SC (36% reduction) obtained from the XRD results [31]. Due to the strong inhomogeneous strain field in closely stacked structures, it is possible to affect the QD coupling probability with the spacer thickness of the SC layers ranging from 15 to 25 nm.

4. Device application of QDs with GaP SC

In this section, device applications of the SC technique including lasers and modulators are reported. The QD long-wavelength emission using MOCVD has been more difficult due to the accumulation of the overall compressive strain by stacking In(Ga)As/GaAs QDs, which results in the formation of threading dislocations and increases the internal loss due to scattering introduced by undulation of the interface between the active region and the p-cladding layer [42, 43]. Only recently has the ground-state lasing at $\lambda > 1.24\,\mu$m from MOCVD-grown stacked QDs been demonstrated [21–23, 25]. To date, there are several approaches to demonstrate the ground state lasing grown by MOCVD. Kim *et al* has embedded the QDs in an InGaP barrier [21], which results in high $T_0 = 210$ K and $J_{th} = 200$ A cm^{-2} at $\lambda = 1.28\,\mu$m. Kaiander *et al* and Tatebayashi *et al* have employed annealing steps that remove defect clusters [22, 23] resulting in a low transparency current density of 7.2 A cm^{-2} per QD layer at $\lambda = 1.265\,\mu$m. Guimard *et al* have introduced antimony-surfactant-mediated growth methods to increase the QD density and improve the QD uniformity, resulting in the ground-state RT lasing under cw operation at 1.35 μm with a maximum modal gain of 19.3 cm^{-1}. The SC technique proposed in this paper may be a powerful tool to circumvent the formation of threading dislocations and reduction in the dot density caused by the accumulative compressive strain to improve the device performance including the modal gain and the internal loss.

4.1. *Growth of device structures by MOCVD*

The QD laser structure and modulator are grown on a (1 0 0) n-GaAs substrate followed by a 1.46 μm n-$Al_{0.3}Ga_{0.7}As$ cladding layer, an active region, a 1.46 μm p-$Al_{0.3}Ga_{0.7}As$ cladding layer and a 400 nm p$^+$-GaAs contact layer. The growth temperatures of n- and p- cladding layers are 700 and 560 °C, respectively. The active region consists of six stacks of InAs QDs with GaP SC layers. Each QD layer is grown at 520 °C on a 5 ML $In_{0.15}Ga_{0.85}As$ buffer and covered with a 25 ML $In_{0.15}Ga_{0.85}As$ cap. The growth rate of InAs QDs is 0.075 ML s^{-1}, and the nominal thickness of InAs is approximately 2.6 MLs. The density of the 1st and 4th layers of InAs QDs is 1.9×10^{10} cm^{-2} and 2.0×10^{10} cm^{-2}, respectively, as shown in figure 9(*a*), which indicates that the density of each layer remains constant throughout the QD stacking process due to the effect of SC. In the growth of stacked

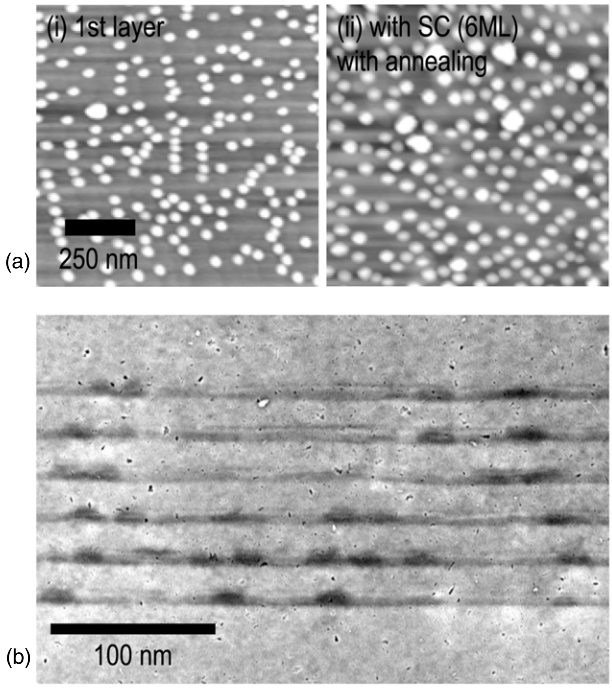

Figure 9. (*a*) AFM images of the uncapped surface of (i) a single layer (dot density: 1.9×10^{10} cm^{-2}), (ii) the fourth layer of stacked InAs QDs containing a 6 ML GaP SC layer with indium flushing (2.0×10^{10} cm^{-2}). (b) Cross-sectional TEM image of six layers of InAs QDs embedded in an $In_{0.15}Ga_{0.85}As$ layer with 27 nm spacing containing 6 ML GaP SC layers [25].

QDs, an *indium-flushing* method [44] is used to improve the surface morphology and the quality of the GaAs capping layer [22, 23, 33]. An *indium-flushing* step is accomplished by annealing the surface for 300 s under the AsH_3 flow after the QD layer is covered with a 4 nm GaAs cap. Then a GaP SC layer is grown on the GaAs cap. After the growth of the GaP SC layers, the wafer temperature is increased to 540 °C and the surface of GaP is annealed for 180 s under the TBP flow. Both annealing steps aim to improve the interlayer dot uniformity for QDs embedded in GaAs [45, 46]. After surface annealing, another 14 nm GaAs cap is grown at 540 °C. Then the wafer temperature decreases to 520 °C, and the next QD layer is grown. Figure 9(*b*) shows the XTEM image of a six-stack QD active region along with the GaP SC layers and 27 nm spacing. The image suggests that the InAs QDs are not formed in the columnar growth mode as might be expected from the very close QD spacing. Rather, each QD layer nucleates semi-independently of the underlying QD layer as previously discussed.

4.2. QD lasers with GaP SC

Broad area laser structures, with a 100 μm wide ridge and varying cavity lengths, are fabricated for device characterization. First, we measure the spontaneous RT emission spectra of the QD lasers with cavity lengths of 500 μm and as-cleaved facets on both sides. Figure 10(*a*) shows the EL spectra of the QD laser at various injection current densities under pulsed conditions (1% duty cycle) ranging from 20 A cm^{-2} to 2 kA cm^{-2}. We can observe

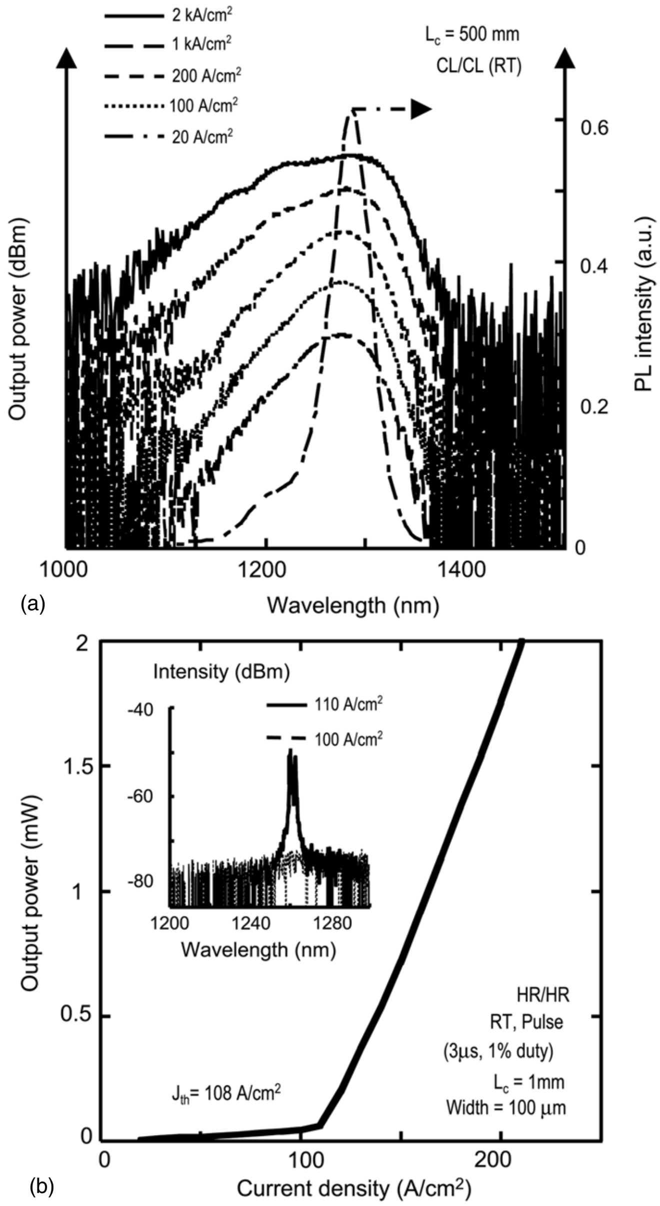

Figure 10. (*a*) EL spectra of 6-stack InAs QD lasers with GaP SC layers at various injected current densities ranging from 20 A cm^{-2} to 2 kA cm^{-2} and the PL spectrum of their active layers. (*b*) *L–I* characteristics of the QD lasers under pulsed operation at RT. A threshold current density J_{th} is 108 A cm^{-2}. The inset shows the EL spectra of fabricated QD lasers just above and below the threshold current J_{th} [25].

separate peaks from the characteristic discrete energy levels of QDs at wavelengths of 1.28, 1.22 and 1.16 μm under high injection currents. The FWHM of the ground-state emission from the PL spectrum with the same active layer is 33 meV. The intersubband energy spacing between the ground and excited states is 48 meV. Moreover, the EL peak of the QD laser does not shift towards a shorter wavelength with the two postgrowth annealing steps as the PL peak of the active region [23]. We then study the output power–current (*L–I*) characteristics and lasing spectra of the laser structure with the cavity length of 1 mm at RT. High-reflectivity coatings (reflectivity: 90 and 94%) are applied on the two facets of the laser structure. Figure 10(*b*) shows the *L–I* characteristics and EL spectra just below and above the threshold current under the same pulsed conditions. The threshold current density, J_{th}, is 108 A cm^{-2} and the lasing wavelength is 1.265 μm. We believe that the lasing wavelength can be extended to 1.3 μm by increasing the indium composition of the InGaAs matrix [12].

The internal loss and modal gain of the QD laser are assessed by the segmented contact method using a single multi-section device [47, 48]. The wafer is processed into a multi-section device, where each section is electrically isolated from every other, following conventional broad area laser processing techniques, as shown in the inset of figure 11(*a*). The width of the stripe is 50 μm. A final multi-section device is composed of 0.3 or 0.6 mm long sections. The EL emission is detected from the cleaved facets of the cavity by using an optical spectrum analyzer. A net modal gain, g, and a modal absorption, α are derived from equations given as [48]

$$g = \frac{1}{L}\ln\left(\frac{I_3 - I_1}{I_2 - I_1} - 1\right), \tag{13}$$

$$\alpha = \frac{1}{L}\ln\left(\frac{I_2 - I_1}{I_{31} - I_1}\right), \tag{14}$$

where L is the cavity length, I_1, I_2, I_3 or I_{31} is the EL intensity when sections 1; 1 and 2, 1, 2 and 3, or 1 and 3, respectively, shown in the inset of figure 11(*a*) are pumped with a current density J. The internal loss is determined to be approximately 5 cm^{-1} from the modal absorption spectrum, derived from equation (13), below the bandgap of the ground state of QDs, as shown in figure 11(*a*). The low internal loss is likely due to the suppression of the overall compressive strain by inserting GaP SC layers, resulting in the morphology improvement at the heterostructure interface. We plot the modal gain characteristics of the ground states against the injected current densities as shown in figure 11(*b*), and the net gain spectra are derived from equation (14) and shown in the inset. By increasing the injected current density, the modal gain of the ground state first increases and then saturates. We can estimate that the maximum modal gain of the ground state of the QD laser is approximately 10 cm^{-1}. It is possible to obtain higher modal gain by increasing the stacking numbers because we can form stacked QDs without reducing the dot density caused by the accumulated strain field when stacking QDs by inserting SC layers within the stacked structure.

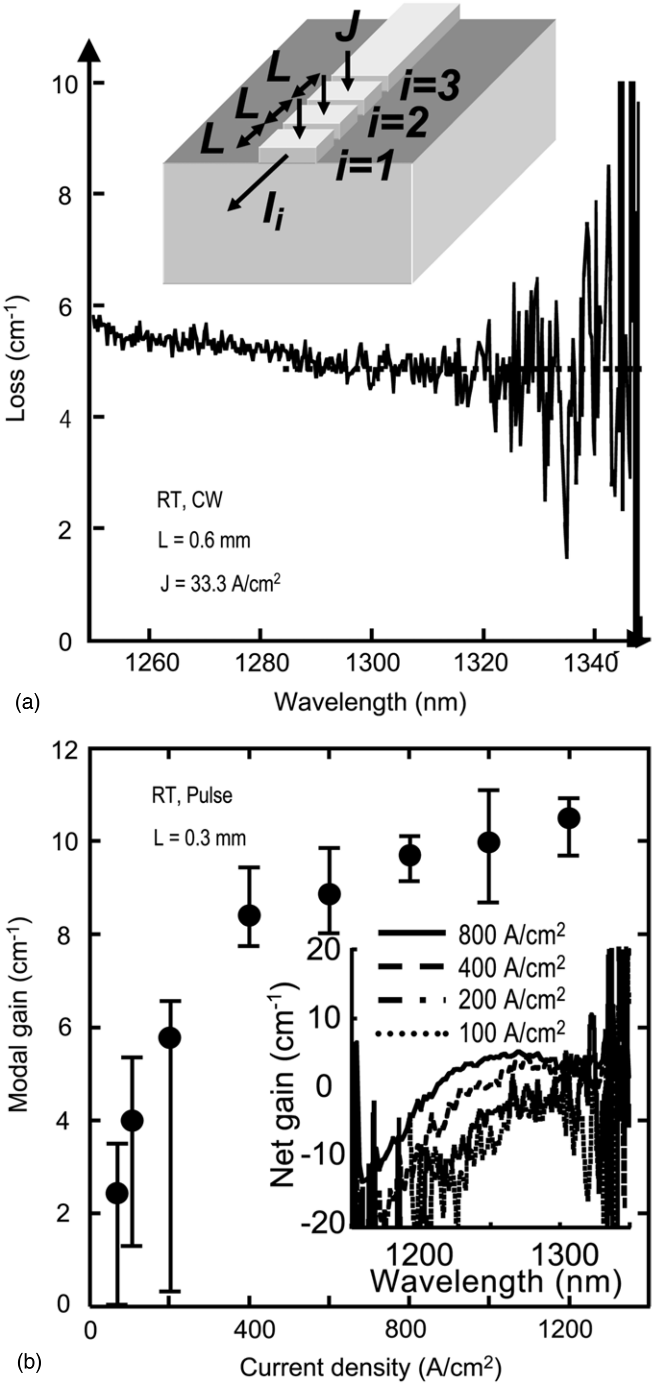

Figure 11. (*a*) The modal absorption spectrum of the fabricated QD lasers under an injected current density (J) of 33 A cm^{-2}. The inset shows the schematic diagram of a multi-section device structure. (*b*) The modal gain of the ground state of the stacked InAs QD lasers against the injected current densities. The inset shows the net gain spectra of the QD lasers at various injected current densities ranging from 100 to 800 A cm^{-2} [25].

4.3. QD modulators with GaP SC

QD-based EO modulators have attracted considerable interest for their potential application to monolithic photonic devices integrated with other components under a low-driving voltage owing to their enhanced optical nonlinearities and EO properties. These enhancements are due to the enhancement of the oscillator strength [49–51] caused by the complete confinement of electrons and holes within discrete sets of the density of states [1]. So far, several groups have reported the measurement of the phase retardation characteristics of single layer self-assembled In(Ga)As/GaAs QDs emitting at 1.0–1.05 μm [52–54] and showed much higher LEO and QEO coefficients than the GaAs bulk material at a pumping wavelength of 1.15 μm [53, 54]. However, there has been few reports of QD modulators operating at 1.3 μm which is technically suitable for fibre-optic communication systems [55].

Measurement of the EO coefficients is performed by coupling light from a distributed feedback laser onto one

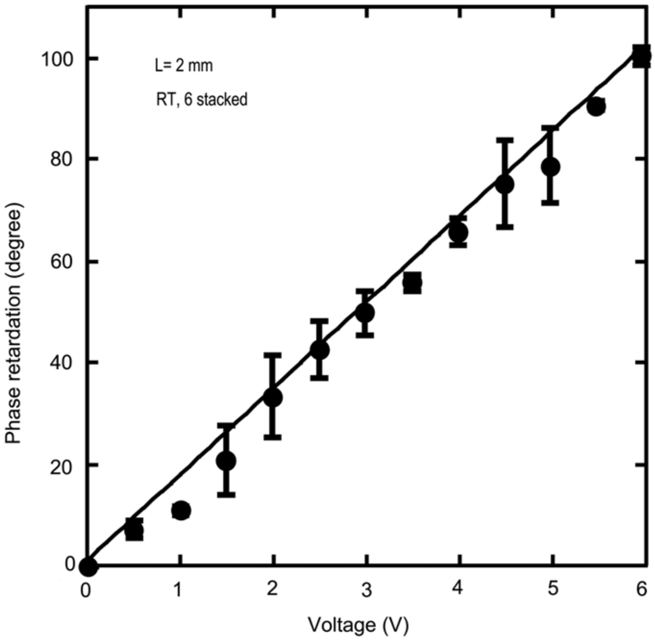

Figure 12. Phase retardation characteristics of 6-stacked InAs quantum dot modulators with a 2 mm cavity length under a reverse bias voltage. The solid line is a fit to the measured data [55].

facet of the previously mentioned 5-stack QD modulator/laser structure with a cavity length, L, of 2 mm by using an objective lens. The wavelength of the pumping laser, λ, is 1.35 μm, detuned by 50 meV from the ground state of QDs. The polarization of the pumping laser is oriented through the use of an input polarizer at 45° in the direction of the electric field applied to the device. The phase retardation of the output light from the propagation through the device is measured with an analyzer with a Ge detector and a lock-in amplifier.

Figure 12 shows the phase retardation characteristics of the QD modulator device as a function of the reverse bias voltage. The LEO and QEO are obtained by fitting the measured phase retardation, $\Delta\Phi$, with the relation [56]

$$\Delta\Phi = \frac{\pi L n_0^3}{\lambda}(\Gamma_1 r E + \Gamma_q s E^2), \tag{15}$$

where n_0 is the effective refractive index in the active region, E is the electric field in the active region derived from the standard depletion model, r and s are the LEO and QEO, respectively, and Γ_1 and Γ_q are the linear and quadratic confinement factors of the waveguide. Both LEO and QEO have two contribution components, the QDs and the GaAs matrix:

$$\Gamma_{1(q)} r(s) = \Gamma_{1(q)} r(s)_{QD} + \Gamma_{1(q)Matrix} r(s)_{Matrix}, \tag{16}$$

where $\Gamma_{1(q)QD}$ and $\Gamma_{1(q)Matrix}$ are the confinement factors of the QDs, taking into account the fill factor, and the GaAs matrix, and $r(s)_{QD}$ and $r(s)_{Matrix}$ are the LEO (QEO) of the QDs and the GaAs matrix, respectively. The fill factor of the QD layer is estimated to be 0.063 by using the technique described in [57]. The optical confinement factors are evaluated from the optical mode distribution and $\Gamma_{1(q)QD}$ and $\Gamma_{1(q)Matrix}$ are 1.27×10^{-3} and 0.559, respectively. The r_{GaAs} and s_{GaAs} are given by 1.6×10^{-12} m V^{-1} and 1.3×10^{-20} m^2 V^{-2} at 1.3 μm, respectively, from [58]. The LEO and QEO of InAs QDs, r_{QD} and s_{QD}, can thus be derived from the measured data, fitted by the equation of the relationship between the phase retardation and the applied electric field shown above, to be 2.4×10^{-11} m V^{-1} and 3.2×10^{-18} m^2 V^{-2}, respectively. Both these values are larger than those of GaAs bulk, and LEO of InAs QDs is comparable to that of lithium niobate ($\sim 3.1 \times 10^{-11}$ m V^{-1}).

From equations (15) and (16), phase retardation characteristics largely depend on the optical confinement factor of QDs and the electric field applied to the active region. It would be possible to obtain larger phase retardation under a lower bias voltage by stacking QDs as many layers as possible in order to increase the optical confinement factor. It is also beneficial to stack QDs more densely to obtain a higher applied electric field if the modulator is operated under the same applied voltage. The use of GaP SC can enable the growth of dense and uniform QD stacks without any threading dislocations or strain accumulation through the compensation of the overall compressive strain within the active region.

5. Summary

We demonstrate the SC technique for the growth of a stacked InAs/GaAs QD structure. Experimental and mathematical treatments of the reduction of two types of strain, homogeneous and inhomogeneous strain, in the compensated stacked QD structure are conducted. The HRXRD technique is used to quantify the reduction in homogeneous strain, indicating that >36% strain reduction can be accomplished. AFM reveals that the SC layer improves QD uniformity and reduces the defect density. PL characterization is used to quantify the optical property of stacked InAs QDs. The inhomogeneous strain field is investigated by studying the strain coupling probability as a function of the spacer thickness, indicating that 19% reduction in inhomogeneous strain is quantified. This SC technique is shown to improve the material quality with an extremely low defect density and a constant QD density suitable for development of long-wavelength devices on GaAs substrates.

Next, device application of the SC technique, including lasers and modulators, is demonstrated. First, ground-state lasing of stacked InAs/GaAs QDs with a spacer thickness of 27 nm and GaP SC layers of 6 MLs embedded within is demonstrated at RT. The obtained lasing wavelength and the threshold current densities are $\lambda = 1.265$ μm and 108 A cm^{-2}, respectively. From the EL spectra, the observed lasing is shown to originate from the ground state of stacked InAs QDs. We assess the internal loss and modal gain of the structure by using the segmented contact method. The maximum modal gain is approximately 10 cm^{-1}, and the internal loss is as low as 5 cm^{-1}, which is almost comparable to that of QD lasers by MBE. This is promising for applications of light sources in the mid-infrared optical communication system. In addition, the EO properties of InAs/GaAs QDs are reported. The LEO and QEO coefficients are 2.4×10^{-11} m V^{-1} and 3.2×10^{-18} m^2 V^{-2}, respectively, which are significantly larger than those of GaAs bulk materials. Also, the LEO coefficient is comparable to that of lithium niobate.

References

[1] Arakawa Y and Sakaki H 1982 *Appl. Phys. Lett.* **40** 939
[2] Kirstaedter N *et al* 1994 *Electron. Lett.* **30** 1416
[3] Mirin R, Gossard A and Bowers J 1996 *Electron. Lett.* **32** 1732
[4] Shoji H, Nakata Y, Mukai K, Sugiyama Y, Sugawara M, Yokoyama N and Ishikawa H 1996 *Japan. J. Appl. Phys.* **35** L903
[5] Saito H, Nishi K, Ogura I, Sugou S and Sugimoto Y 1996 *Appl. Phys. Lett.* **69** 3140
[6] Kamath K, Bhattacharya P, Sosnowski T, Norris T and Phillips J 1996 *Electron. Lett.* **32** 1374
Sellin R L, Ribbat Ch, Grundmann M, Ledentsov N N and Bimberg D 2001 *Appl. Phys. Lett.* **78** 1207
[7] Mukai K, Ohtsuka N, Sugawara M and Yamazaki S 1994 *Japan. J. Appl. Phys.* **33** L1710
[8] Nishi K, Saito H, and Sugou S and Lee J-S 1999 *Appl. Phys. Lett.* **74** 1111
[9] Ustinov V M *et al* 1999 *Appl. Phys. Lett.* **74** 2815
[10] Mukai K and Sugawara M 1999 *Appl. Phys. Lett.* **74** 3963
[11] Bloch J and Shah J 1999 *Appl. Phys. Lett.* **75** 2199–201
[12] Tatebayashi J, Nishioka M and Arakawa Y 2001 *Appl. Phys. Lett.* **78** 3469
[13] Huffaker D L, Park G, Zou Z, Shchekin O B and Deppe D G 1998 *Appl. Phys. Lett.* **73** 2564
[14] Mukai K, Nakata Y, Ohtsubo K, Sugawara M, Yokoyama N and Ishikawa H 1999 *IEEE Photon. Technol. Lett.* **11** 1205
[15] Liu G T, Stintz A, Li H, Malloy K J and Lester L F 1999 *Electron. Lett.* **35** 1163
[16] Zhukov A E *et al* 1999 *Appl. Phys. Lett.* **75** 1926
[17] Park G, Shchekin O B, Csutak S, Huffaker D L and Deppe D G 1999 *Appl. Phys. Lett.* **75** 3267
[18] Otsubo K, Hatori N, Ishida M, Okumura S, Akiyama T, Nakata Y, Ebe H, Sugawara M and Arakawa Y 2004 *Japan. J. Appl. Phys.* **43** L1124
[19] Eliseev P G, Li H, Stinz A, Liu G T, Newell T C, Malloy K J and Lester L F 2000 *Appl. Phys. Lett.* **77** 262
[20] Passaseo A *et al* 2003 *Appl. Phys. Lett.* **82** 3632
[21] Kim S M, Wang Y, Keever M and Harris J S 2004 *IEEE Photon. Technol. Lett.* **16** 377
[22] Kaiander I N, Sellin R L, Kettler T, Ledentsov N N, Bimberg D, Zakharov N D and Werner P 2004 *Appl. Phys. Lett.* **84** 2992
[23] Tatebayashi J, Hatori N, Ishida M, Ebe H, Sugawara M, Arakawa Y, Sudo H and Kuramata A 2005 *Appl. Phys. Lett.* **86** 053107
[24] Nuntawong N, Xin Y -C, Birudavolu S, Wong P S, Huang S, Hains C P and Huffaker D L 2005 *Appl. Phys. Lett.* **86** 193115
[25] Tatebayashi J, Nuntawong N, Xin Y C, Wong P S, Huang S H, Hains C P, Lester L F and Huffaker D L 2006 *Appl. Phys. Lett.* **88** 221107
[26] Guimard D, Ishida M, Hatori N, Nakata Y, Sudo H, Yamamoto T, Sugawara M and Arakawa Y 2008 *IEEE Photon. Technol. Lett.* **20** 827
[27] Miller B I, Koren U, Young M G and Chien M D 1991 *Appl. Phys. Lett.* **58** 1952
[28] Zhang G and Ovtchinnikov A 1993 *Appl. Phys. Lett.* **62** 1644
[29] Thijs P J A, Tiemeijer L F, Binsma J J M and Dongen T van 1994 *IEEE J. Quantum Electron.* **30** 477
[30] Zhang X Q, Ganapathy S, Kumano H, Uesugi K and Suemune I 2002 *J. Appl. Phys.* **92** 6813
[31] Lever P, Tan H H and Jagadish C 2004 *J. Appl. Phys.* **95** 5710
[32] Nuntawong N, Birudavolu S, Hains C P, Huang S, Xu H and Huffaker D L 2004 *Appl. Phys. Lett.* **85** 3050
[33] Nuntawong N, Huang S, Jiang Y B, Hains C P and Huffaker D L 2005 *Appl. Phys. Lett.* **87** 113105
[34] Van de Merwe J H 1963 *J. Appl. Phys.* **34** 117
[35] Nasi L, Ferrari C, Lazzarini L and Clarke G 2002 *J. Appl. Phys.* **92** 7678
[36] Tersoff J, Teichert C and Lagally M G 1996 *Phys. Rev. Lett.* **75** 1675
[37] Solomon G S, Trezza J A, Marshall A F and Harris J S 1996 *Phys. Rev. Lett.* **76** 952
[38] Xie Q, Madhakar A, Chen P and Kobayashi N P 1995 *Phys. Rev. Lett.* **75** 2542
[39] Nuntawong N, Tatebayashi J, Wong P S and Huffaker D L 2007 *Appl. Phys. Lett.* **90** 163121
[40] Jesson D E, Pennycook S J, Baribeau J M and Houghton D C 1993 *Phys. Rev. Lett.* **71** 1744
[41] Schwoebel R L 1969 *J. Appl. Phys.* **40** 614
[42] El-Emawy A A, Birudavolu S, Wong P S, Jiang Y B, Xu H, Huang S H and Huffaker D L 2003 *J. Appl. Phys.* **93** 3529
[43] Ledentsov N N, Maximov M V, Bimberg D, Maka T, Sotomayor Torres C M, Kochnev I V, Krestnikov I L, Lantratov V M, Cherkashin N A and Musikhin Yu M 2000 *Semicond. Sci. Technol.* **15** 604
[44] Wasilewski Z R, Fafard S and McCaffrey J P 1999 *J. Cryst. Growth* **201/202** 1131
[45] Le Ru E C, Bennett A J, Roberts C and Murray R 2002 *J. Appl. Phys.* **91** 1365
[46] Liu H Y *et al* 2004 *Appl. Phys. Lett.* **85** 704
[47] Thomson J D, Summers H D, Hulyer P J, Smowton P M and Blood P 1999 *Appl. Phys. Lett.* **75** 2527
[48] Xin Y-C *et al* 2006 *IEEE J. Quantum Electron.* **42** 725
[49] Schmitt-Rink S, Miller D A B and Chemla D S 1987 *Phys. Rev.* B **35** 8113
[50] Takagahara T 1987 *Phys. Rev.* B **36** 9293
[51] Bryant G W 1988 *Phys. Rev.* B **37** 8763
[52] Davis L, Ko K K, Li W -Q, Sun H C, Lam Y, Brock T, Pang S W and Bhattacharya P K 1993 *Appl. Phys. Lett.* **62** 2766
[53] Qasaimeh O, Kamath K, Bhattacharya P and Phillips J 1998 *Appl. Phys. Lett.* **72** 1275
[54] Ghosh S, Lenihan A S, Dutt M V G, Qasaimeh O, Steel D G and Bhattacharya P 2001 *J. Vac. Sci. Techonol.* B **19** 1455
[55] Tatebayashi J, Laghmavarapu R B, Nuntawong N and Huffaker D L 2007 *Electron. Lett.* **43** 410
[56] Bloemer M J and Myneni K 1993 *J. Appl. Phys.* **74** 4849
[57] Kamath K, Phillips J, Jiang H, Singh J and Bhattacharya P 1997 *Appl. Phys. Lett.* **70** 2952
[58] Lee S S, Ramaswamy R V and Sundaram V S 1991 *IEEE J. Quantum Electron.* **27** 726